On the Improvement of VCO Based Matrix Particle Detector for High Resolution Particles Recognition and Tracking

K. Coulie, W. Rahajandraibe, Laurent Ottaviani

On the Improvement of a VCO Based Matrix Particle Detector for High Resolution Particles Recognition and Tracking

K. Coulié, W. Rahajandraibe and Laurent Ottaviani

***Abstract*— A particle detection chain based on a CMOS-SOI VCO circuit associated to a matrix of detection is presented. The solution is used for the recognition and tracking of an alpha particle.**

***Index Terms*— Sensor, detection, VCO, radiation**

I. Introduction

SEMICONDUCTOR radiation detectors, also called solid-state detectors, can be classified into several categories, depending on the application field and the particles to be detected. These detectors are based on charge collection and amplification using a semiconductor volume such as a p-n junction [1-2]. They exhibit several advantages in comparison with other types of detectors such as gas-filled counters. For instance, they usually offer faster charge-collection time which provide the ability to process higher counting rates. Another advantage is their compactness which allows the measurement of intensity variations over small distances improving the measurement resolution. A pixel organization including several sensors could be used when a high detector sensitivity is required [2-8]. This case will be investigated in this work.

Particles counting and/or recognition require the conditioning of the signal generated by the sensor. Most of the existing conditioning chains are based on a direct reading of the detected currents created by the crossing of an ionizing particle through the matter. When an embedded reading system is necessary, this solution could not be suitable for the detection of low energy particles where the current signature could be a narrow pulse with a duration of few nanoseconds. Indeed, the readout chain must ensure sufficiently high resolution (optimized Signal-to-Noise-Ratio) for an appropriate post-processing. Moreover, a reading amplifier exhibiting a fast response time is required which means a higher current consumption and complex circuit implementation. Designing high precision, low-power wideband amplifier is a critical issue. As a consequence, most practical detectors are based on direct reading of the detected currents using Charge Sensitive Amplifiers (CSA) [9]. In this case, the circuit delivers a limited amount of information on the actual current shape and no information about the electrical signature of the particles is available. In applications such as gas prospection or medical therapy, the characteristics of the electrical signature of the particles must be known. Moreover, the knowledge of the generated current shape at the output of the detector allows easier post processing of the signal.

In this context, a new approach based on the use of a ring oscillator was developed with an innovative conditioning method [10]. This new approach is based on the reading of the information related to indirect output parameters of the detection chain signal (i.e. voltage variation), instead of directly measuring the current from the sensor. This solution avoids most of the design problems described upper. Then, the information is extracted by correlating the initial oscillating signal of the system with the oscillating signal after the particle has passed the detector. The only requirement to allow particle recognition is then to link the output information (i.e. voltage variation of the oscillating signal) to the input information (current stimuli).

The full detection system (VCO + matrix) will be described in section II. Section III is dedicated to the VCO chain calibration which is mandatory for particle recognition. Part IV deals with the optimization of the detection matrix and section V presents two case studies: an alpha particles and an aluminum ion. The last section concludes the paper.

II. Presentation of the Detection System

The proposed detection system is composed of a detection matrix together with an innovative readout circuit based on a high frequency voltage controlled oscillator. The operating is synthesized in this section.

A. The VCO detection chain

The detection chain has been designed and implemented on 130nm CMOS SOI technology, then simulated at circuit level using “Spectre” simulator (SPICE-based) under Cadence *Virtuoso* © CAO tool.

The concept itself was presented in [10-13]. The VCO chain

K. Coulié, W. Rahajandraibe and L. Ottaviani are with Aix-Marseille University, CNRS and University of Toulon, IM2NP UMR 7334, Marseille France (karine.coulie@im2np.fr, wenceslas.rahajandraibe@im2np.fr and Laurent.ottaviani@im2np.fr).

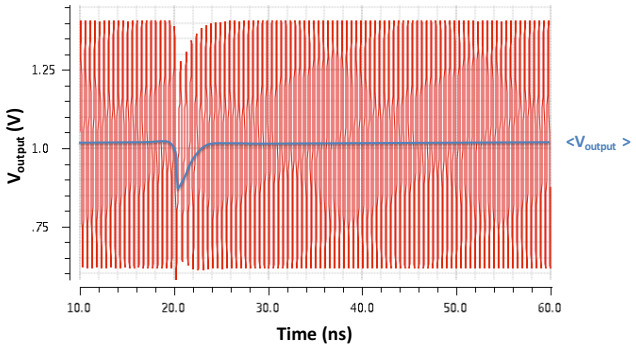

Fig.1. Variation of the output voltage versus time for the indirect detection chain (VCO based).

is composed of three parts: a CMOS based pixel detector, a shaping circuit based on a Voltage Controlled ring Oscillator (VCO) and a system for frequency and amplitude detection (Fig. 1). This system allows the evaluation of the circuit sensitivity to radiation by measuring the oscillator responses. In the very first versions of the system, the operating frequency of 0,35µm Bulk Silicon substrate CMOS VCO was 1MHz. Thanks to a new solution based on another CMOS process (130nm SOI), it reaches now 4.3GHz. This increase of the operating frequency makes possible the development of new methods for signal recognition. As actual operating frequencies are reaching 4.3GHz, the shape of the signal is directly reproduced at the output of the VCO. Then, the output parameters are now the frequency variation along the time and the average voltage variation (Fig.1). The advantage of this solution is a direct recognition of the signal shape as an amplitude modulation of the VCO output frequency.

B. The detection matrix

In order to improve the efficiency of the detection and the tracking ability, a *N*x*M* matrix is modeled and analyzed (Fig.2 and 3). The input current is no longer the simplified current used for the VCO characterization. Now, the current source comes from the realistic simulation of the matrix using TCAD device simulation tools (Synopsis ©). The effect of the ion strike is simulated using the *Heavy Ion* module of Synopsis [14], considering an electron-hole pair column centered on the ion track axis. The Linear Energy Transfer is defined as the energy lost by the particle, by unit of length and varies along the track depending on the initial energy of the particles [15]. Depending on the phenomena to be highlighted in this paper, we use a constant or a realistic LET. Thus, for some specific studies, an actual variation of the LET was integrated in our simulations, based on the value given by SRIM tables [16]. As this detector should be suitable for low energy particles detection, the simulated ion is an alpha particle crossing the device with an initial energy of 0.6MeV, which corresponds to a range of 2.3µm in the silicon matrix . The aim is to study the end of the path corresponding to an alpha particle of 1.47MeV generated by the initial interaction of thermal neutron with boron-10. The case of a more energetic particle will also be considered. This is a 50MeV Aluminum which could be procuded by the interaction of fast protons with silicon, for instance [17].

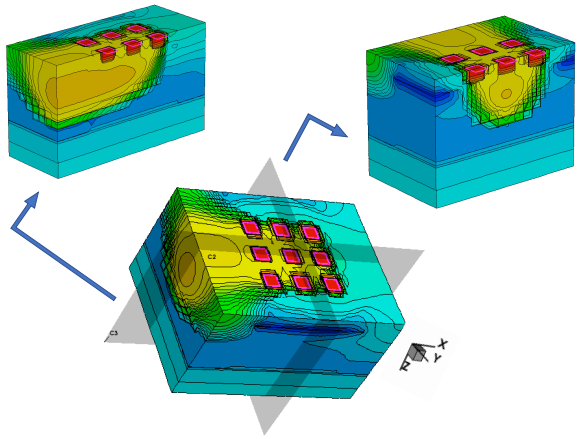

Fig.2. 3D center: simulation of the 3x3 matrix, left: Y-cut and right: X-cut of the matrix.

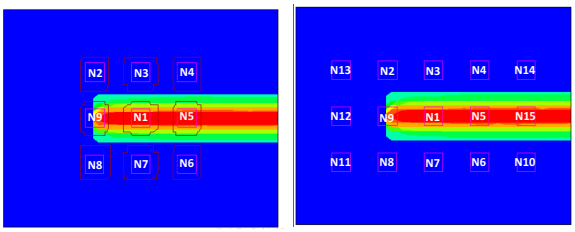

(a) *(b)*

Fig.3. Top view of (a) the nine contacts matrix, (b) the fifteen contacts matrix for the simulation of the alpha particle.

The generation of such a particle in the whole structure is shown in Fig. 2. The particle is generated at 50ps. The currents generated by the particle crossing are shown in Fig. 10 at each electrode. The two structures, 3x3 and 5x3 matrix, are presented in Fig. 3.

III. CALIBRATION OF THE VCO CHAIN

The key point is how the output parameters of the VCO chain can give information related to the input current. This could be done through the analysis of various characteristics extracted from the average voltage variation (Fig. 1). In this paper, we study the variation of the average output signal (ΔV_{max}) versus the maximum of the input current (I_{max}) for different particle charges. In [18], a linearity curve linking input to output parameters was determined for a 2GHz VCO. A new linearity curve has been obtained for this new 4.3GHz VCO (Fig. 4). In [13], it has been demonstrated that two different currents with the same maximum value get the same corresponding ΔV_{max}. Then ΔV_{max} does not depend on the shape of the current but only on the current peak. Thus the measurement of ΔV_{max} appeared to be a reliable parameter to recognize the current peak of the input signal. Through calibration curves, the output parameters can be linked to the input currents, which could allow the incoming particle identification.

To get reliable results, the resolution of the system has to be checked. Thus, the results are valuable if the points are included in the “good detection” zone. This zone corresponds to a linear response of the system in the range ±10 %. When the results are situated out of this zone, the resolution is clearly degraded [18] and the pulse characteristics are also not suitable with the

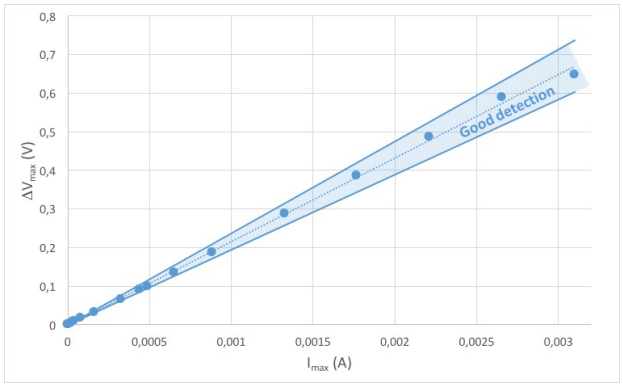

Fig.4. Variation of the average output signal (ΔV_{max}) versus the maximum of the input current (I_{max}).

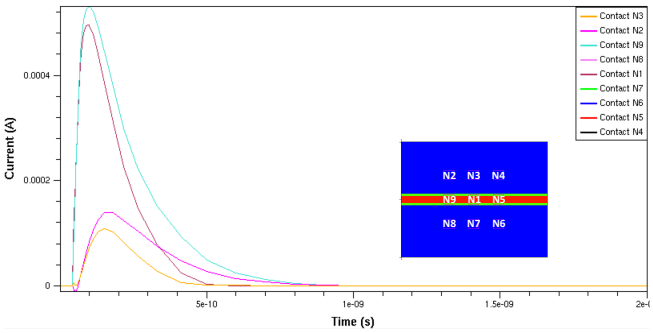

Fig.5. 3x3 matrix. Comparison of currents at the nine contacts, LET=0.07pC/µm, space=0.5µm, depth=0.8µm.

resolution of our system. In this condition the system can only be used as a particle counter.

IV. Optimization of the Detection Matrix

A. *Study of various parameters for the matrix optimization*

This work has been performed for a constant LET. Note that if the approximation of a constant LET is sometimes reasonable, it is not realistic. However the advantage is to uncorrelate the following analysis from LET variation considerations. For this study, the particle crosses entirely the structure, in the Y direction at *depth*=0.8µm as shown in the inset of Fig.5. Then N2, N4, N6, N8 currents are exactly the same because of the symmetry of the matrix. N3/N7 and N9/N5 are also the same for this reason. Then only four currents are characteristics of the cell (Fig.5): N2/N4/N6/N8, N3/N7, N9/N5 and N1.

Various parameters characterizing the detection matrix have been studied. One is the distance between two collection zones, named *space*. The current for two values of "space" are plotted in Fig.6. For *space*=1.2µm the N1 current is higher than for *space*=0.5. For the N3/N7 contacts, which are further from the track, the currents are higher for *space*=0.5 than for *space*=1.2µm. Indeed, the current sharing depends on the distance between contacts. For *space*=1.2µm, the variation of the currents between contacts is higher than for *space*=0.5µm. However, as expected, the total collected charge at the nine contacts, is the same for the two values of space. This charge corresponds to the addition of the integrated current at each contact. The deposited charge is the same for the two *space* parameters. Despite different ways of collection, so different currents at each contacts, the whole collected charge remains the same.

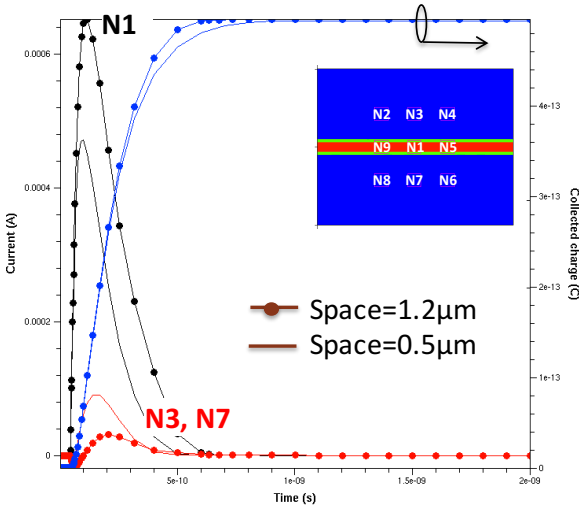

Fig.6. 3x3 matrix (9 contacts). Comparison of currents for N1, N3 and N7 contacts (left) and total collected charges at the nine contacts (right), for two values of the "space" parameter.

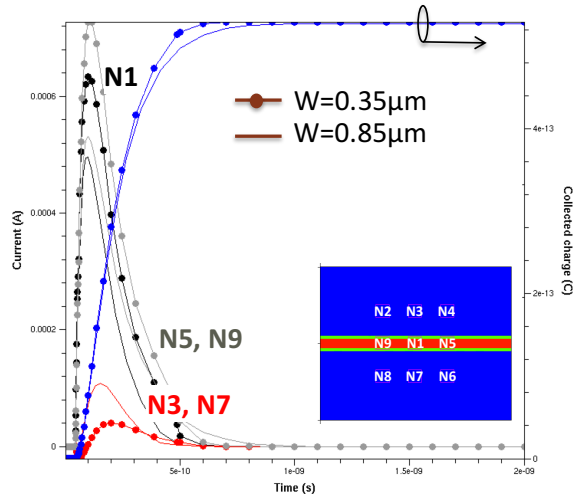

Fig.7. 3x3 matrix (9 contacts). Comparison of currents for N1, N5, N9, N3 and N7 contacts (left) and total collected charges at the nine contacts (right), for two values of the "width" parameter.

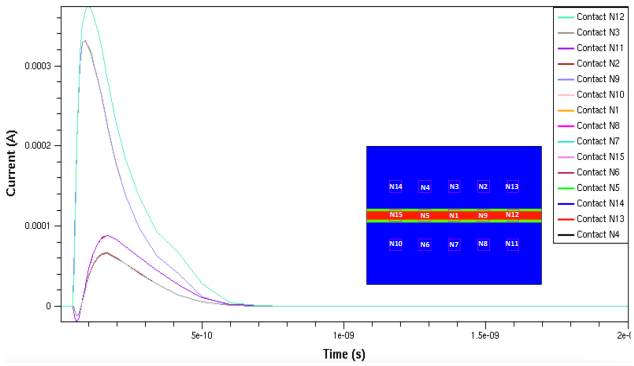

Fig. 8. 5x3 matrix. Comparison of currents at the fifteen contacts, LET=0.07pC/µm, space=0.5µm, depth=0.8µm.

On Fig. 7, we vary the width of the pixels. As for the *space* parameter, increasing the size of the pixels increases the gap between the currents. As the detection efficiency of the VCO depends on the current duration and peak, a configuration inducing a tighter distribution of the characteristics of the

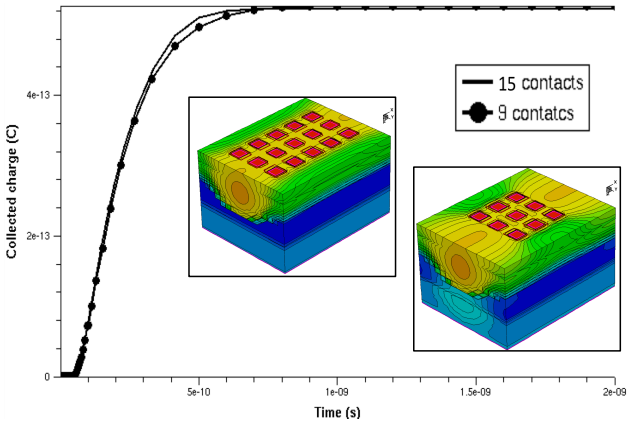

Fig. 9. Comparison of total collected charges at the nine contacts (3x3 matrix) and at the fifteen contacts (5x3 matrix).

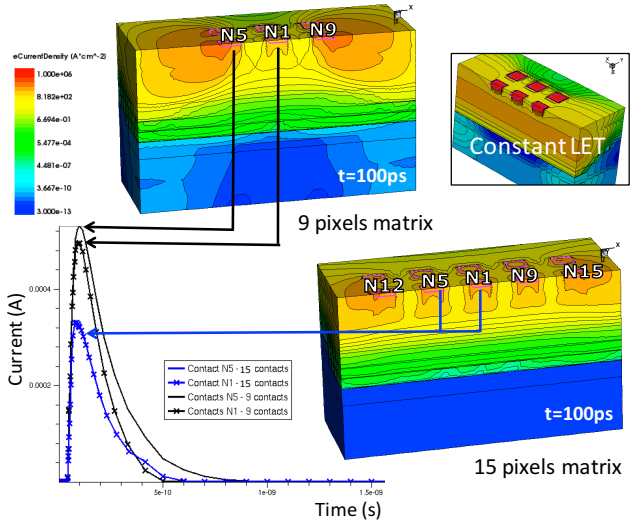

Fig. 10. Comparison of N1 and N5 currents of the 3x3 and 5x3 matrix, LET=0.07pC/µm, space=0.5µm, depth=0.8µm.

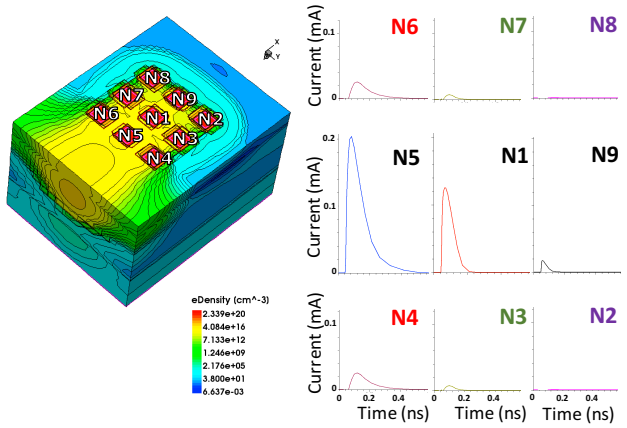

Fig. 11. Current versus time for an alpha particle crossing the nine contacts matrix.

currents would be preferable. Too weak or too short currents could be difficult to be detected by the oscillator. Reducing the gap between the current should increase their probability to be detected.

B. Comparison between a 3x3 and a 5x3 matrix

The currents generated in the 5x3 matrix are plotted in Fig.7 for a constant LET in the same conditions as Fig.5. As for the 3x3 matrix, N10/N11/N13/N14, N2/N3/N4/N6/N7/N8, N9/N1/N5 and N12/N15 are the same currents so four currents can characterize the matrix. The current sharing between the contacts is different in the 5x3 matrix. All the currents are lower in this matrix because 15 contacts are collecting the charge instead of only nine in the 3x3 matrix. In Fig. 9, we checked the value of the total collected charge. As the silicon volume of collection is the same, the total collected charge at the contacts is the same in the two matrixes. The collected charge can give an important information about the deposited energy.

In Fig.10, we consider the case of a constant LET in two matrixes. In the 15 pixels' cell, the currents corresponding to contacts N1 and N5 are the same. It was expected because the charge deposited under the contacts are exactly the same. This case corresponds to the blue currents. In the 9 contacts cell, the charge deposited under contact N5 and contact N1 is also exactly the same. However, the currents issued from 9-pixel matrix (in black in the graph) are more important than from 15-pixel one. This result is due to the effect of the surrounded contacts. Indeed, in the 5x3 matrix, the N1 and N5 contacts are surrounded by 8 contacts. In the 3x3 matrix, the N1 contact is surrounded by 8 contacts whereas the N5 contacts is surrounded by 5 contacts. Then charge sharing is different for the two configurations. This analysis explains the lower value of the current at the N1contact and demonstrates the effect of the adjacent contacts.

V. CASE STUDY

A. Horizontal case study in the middle of the matrix

1) Tracking of an alpha particle

We have tested its response for an alpha particle crossing the 3x3 matrix as shown in Fig.11, with *space*=0.5µm (0.8µm under the contacts). On the left, the electron density corresponding to the crossing of the alpha particle is visible. The currents generated at the 9 pixels are plotted on the right. By comparing red (N6, N4), green (N7, N3) and purple currents (N8, N2), the symmetry of the track is visible. The currents of the middle contacts depict directly the charge density as they are located just above the trace of the ion. This behavior is clearly visible if we have a look at the electron density (Fig. 12). The highest current (N5) corresponds to the highest electron density and the lowest current (N9) corresponds to the lowest charge density. Thus the current variation can provide an information about the charge density in the detection cell.

The current shape can also give information about the distance between the charge generation and the contact (Fig.13). Indeed, the current corresponding to contact N9, appears earlier than the one corresponding to contacts N6 and N4. Contact N9 is located just above the ion whereas the others are on the left and on the right side of the trace.

In [18], the limits of the VCO were tested. Unfortunately, the resolution of our system was not good enough to allow a good detection of the currents generated by the detection cell. This was expected because the duration of the signal was about 0.4ns, which corresponds to an input signal frequency of

2.5GHz, too fast to be detected by a 2GHz oscillator. Thus, the I_{max}-ΔV_{max} couple of the highest current was clearly out of the detection zone which means that the other lower currents are also out of this zone. The VCO frequency now reaches 4.3GHz. Then, in order to test the suitability of the studied VCO to our

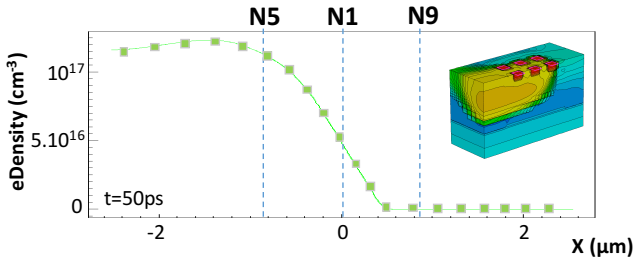

Fig. 12. Electron density versus X direction – alpha particle case.

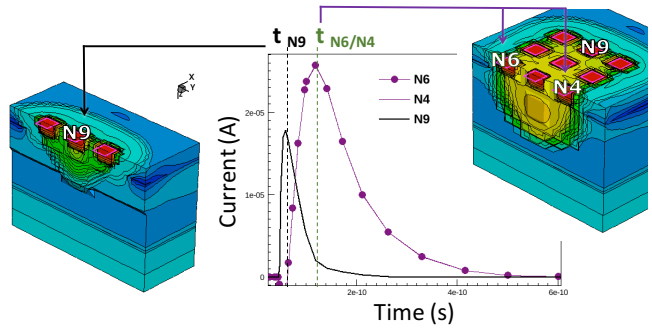

Fig. 13. Current versus time at three contacts: N9, N6 and N4 – alpha particle case.

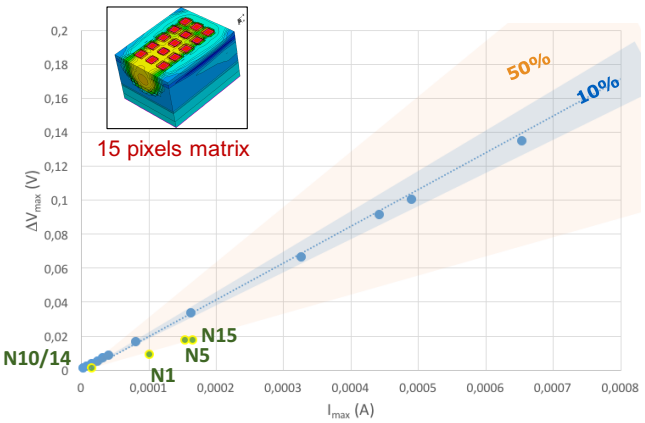

Fig. 14. Linearity curve and four highest currents detected concerning an alpha particle crossing.

detection cell, the crossing of the alpha particle in a 5x3 matrix has been simulated. All the currents of the matrix, generated using Synopsis have been injected in the fifteen VCOs contacts. The results of the four highest currents are plotted on the linearity characteristic of the 4.3GHz VCO (Fig.14). Three of the four points are out of the good detection zone and the others are too low to be detected, however the trend is respected: a higher maximum current corresponds to a higher voltage variation. Only the 4 highest currents are detected but this is enough to get an idea of the particle path making the tracking possible.

2) Tracking of an aluminum ion

The second case study deals with the crossing of an aluminum particle in the 3x3 pixels structure. In Fig. 15 on the right, the orange curves correspond to the currents at the 9 contacts and the blue curves to the average voltages at the output of the voltage controlled oscillator, . The behavior of the blue curves is similar to that of the orange curves which means that the VCO detects all the variations of the input currents.

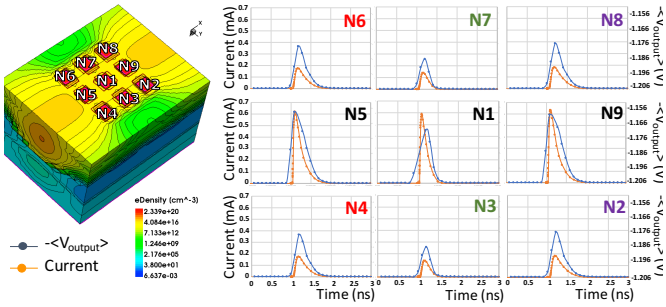

Fig. 15. Current (left scale) and voltage (right scale) versus time for an aluminum ion crossing the nine contacts matrix.

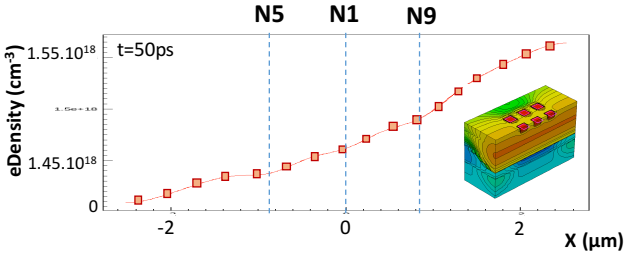

Fig. 16. Electron density versus X direction – aluminum ion case.

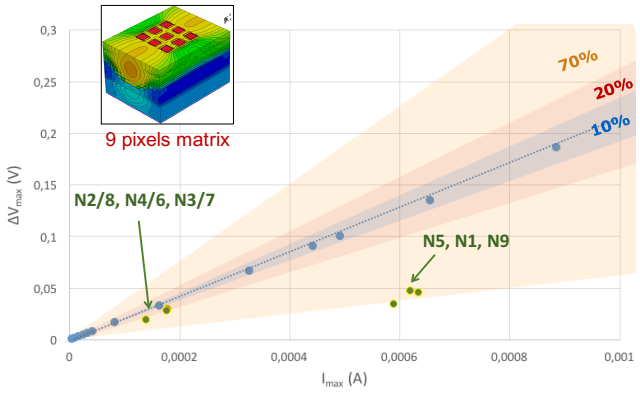

Fig. 17. Linearity curve and detected currents concerning an aluminum ion crossing in a nine contacts matrix.

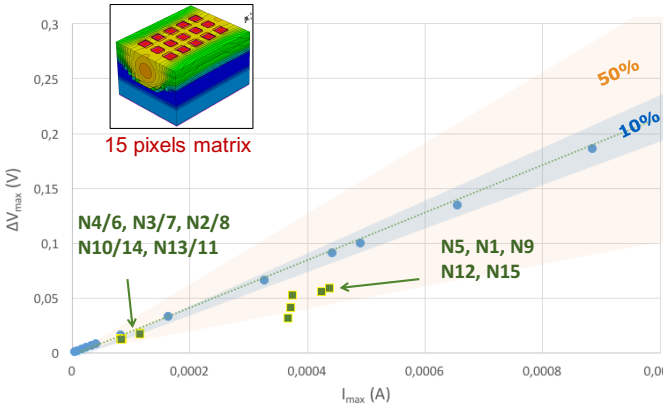

Fig. 18. Linearity curve and detected currents concerning an aluminum ion crossing in a fifteen contacts matrix.

In the X direction, the symmetry of the track can be seen by comparing the red contacts (N6, N4), the green contacts (N7, N3) and purple contacts (N8, N2) (top and bottom graphs). Their currents are clearly the same. The currents corresponding to the black contact is higher because it is located just above the ion. As in the alpha case study, we had a look at the charge density (Fig.16). Comparing the currents at the contacts just above the ion, we were expected an increasing current from the N5 to the N1 contact. However, the N1 contact exhibits a current lower than expected whereas the behavior of contacts N5 and N9 fit with previous observations. This unexpected behavior can be explained by the effect of the surrounded contacts explained in section IV. This influence applies to the case the aluminum crossing the detector.

The currents generated by crossing of the aluminum in the 3x3 matrix have been simulated and the currents were injected at the input of the oscillator (Fig. 17). As for the alpha particle, the maximum of the average voltage versus the current peak is plotted on the linearity curve of the VCO. This time, as the LET and the range of the simulated aluminum is higher, the 9 currents are detected. The shortest currents correspond to contacts just above the track. Their detection is less accurate but the trend is kept: the highest currents exhibit the highest ΔV_{max}.

As previously shown, the detection should be better in a 5x3 matrix. The simulation of the aluminum crossing a 15-pixel cell clearly confirms this assumption (Fig.18). All the currents are detected, the trend is preserved and even for the shortest currents, the detection margin is lower than 50%. This is an encouraging result concerning the ability of the matrix to track various kinds of particles.

B. Diagonal case study in the middle of the matrix

The last part of the study deals with the case of a particle crossing diagonally at depth=0.8µm.

1) Tracking of an alpha particle

The first particle is the alpha particle. Fig. 19 presents the electron density at depth=0.8µm. The local electron density is presented in Fig. 20 for t=50ps, which corresponds to the maximum time of the generation.

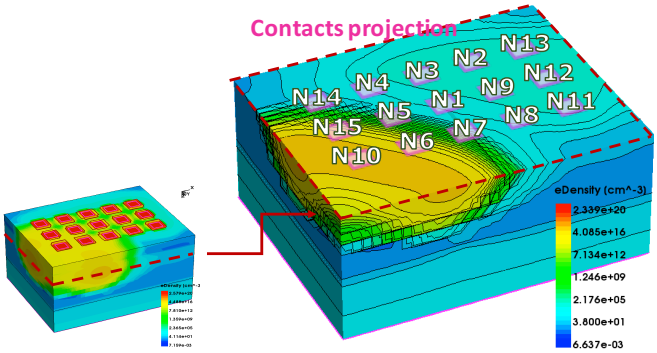

Fig. 19. Alpha generation in the 15-pixels matrix. The figure on the right is a cut at depth=0.8µm. The represented contacts are a projection of the fifteen top contacts.

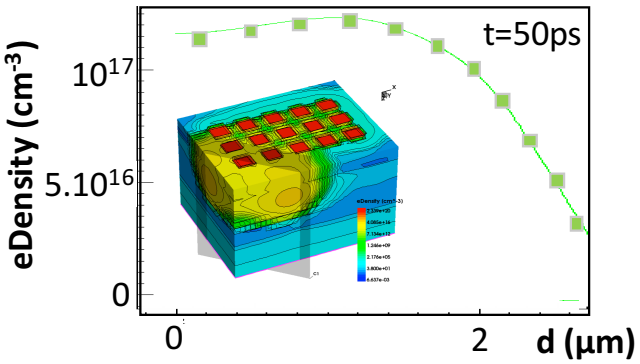

Fig. 20. Electron density along the particle track for the alpha particle.

The three highest currents collected during the particle crossing are shown in Fig.21. The highest current corresponds to N10. This contact is just under the particle track. The maximum of the generation appears at t=78ps. The two other currents correspond to the N6 and N15 contacts. They are approximatively at the same distance from the trace. This is visible through the maximum generation time which is the same for the both contacts: 96ps. As the electron density follows a bell curve, the electron density is almost the same at both contacts. The total current density is shown in Fig. 22. The same variation is observed. By analyzing the maximum current and the maximum generation time, the particle crossing can be approximatively determined. The maximum generation time gives an idea of the distance between the ion and the contact. Then thanks to Fig. 21, we know that the N10 contacts is closer from the particle than the N6 and N15 contacts.

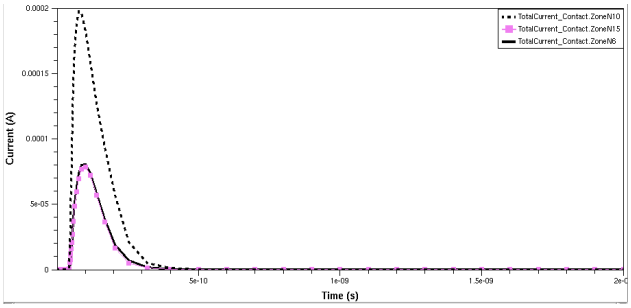

Fig. 21. 5x3 matrix (15 contacts). Comparison of the currents of the three highest currents (N10, N15, N6 contacts) for the alpha particle.

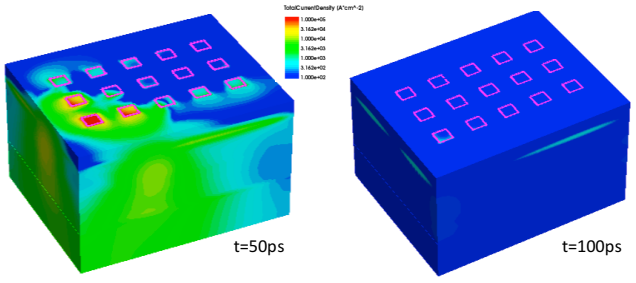

Fig. 22. Total current density at t=50ps (maximum of the generation) and t=100ps for the alpha particle.

2) *Tracking of an aluminum ion*

The same configuration is studied with the aluminum ion. As for the alpha particle, Fig. 23 presents the electron density at depth=0.8µm. The local electron density is presented in Fig. 24 for t=50ps, which corresponds to the maximum time of the generation.

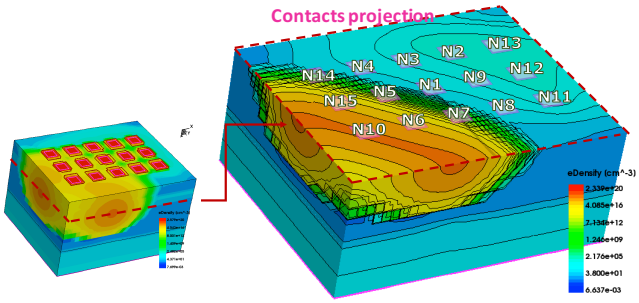

Fig. 23. Aluminum generation in the 15-pixels matrix. The figure on the right is a cut at depth=0.8µm. The represented contacts are a projection of the fifteen top contacts.

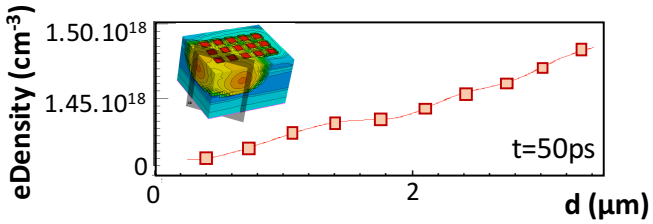

Fig. 24. Electron density along the particle track for the aluminum particle.

The six highest currents collected during the particle crossing are shown in Fig.25. The highest current corresponds once again to N10. As for the alpha particle, this contact is just under the particle track. The maximum of the generation appears at t=108ps. Two other currents correspond to the N6 and N15 contacts. The maximum time corresponding to these currents are again the same 138ps. The N6 current is higher because the local electron density increases along the track (Fig. 24). The N14 and N5 currents are the same and seems to be at the same distance from the track. However, a highest current would have been expected for N5 because the electron density increases along the track. It could be the effect of the surrounding contacts as it has been highlighted in Fig. 10. The N7 current is higher and the its maximum generation time arrives later that for N5 and N14. The N7 contact is probably further from the track. The total current density is shown in Fig. 26. The same variation is observed and visible even at t=100ps.

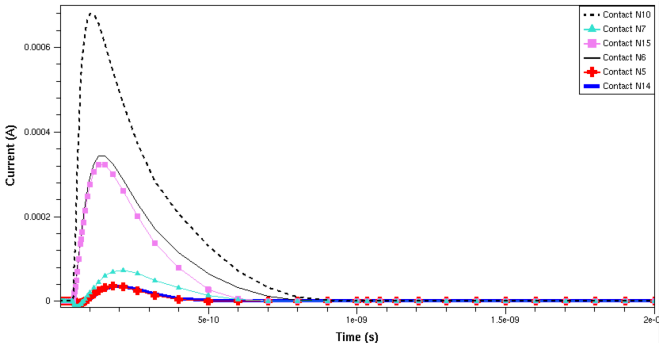

Fig. 25. 5x3 matrix (15 contacts). Comparison of the currents of the six highest currents (N10, N15, N6, N7, N5 and N14 contacts) for the aluminum particle.

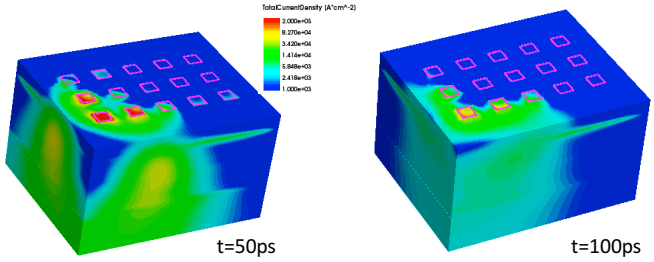

Fig. 26. Total current density at t=50ps (maximum of the generation) and t=100ps for the aluminum particle.

3) *VCO detection*

Both particles have been injected sequentially in the VCO. The average voltage is presented in Fig. 27 for the highest currents corresponding to the two particles.

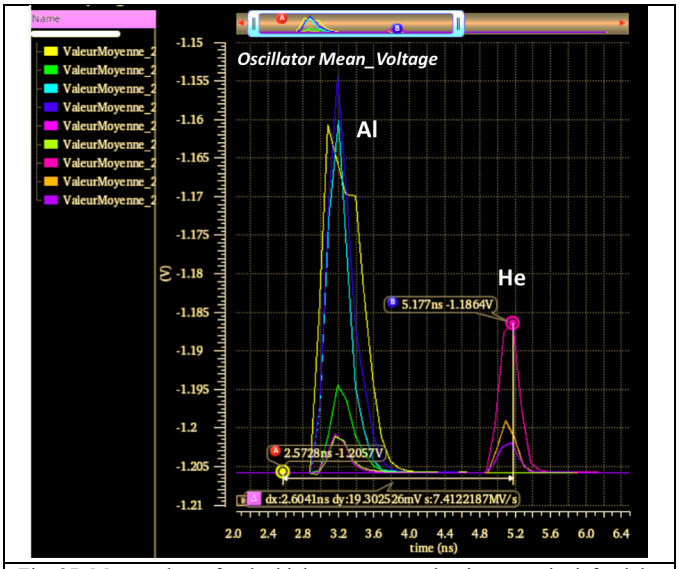

Fig. 27. Mean voltage for the highest currents: aluminum on the left, alpha on the right.

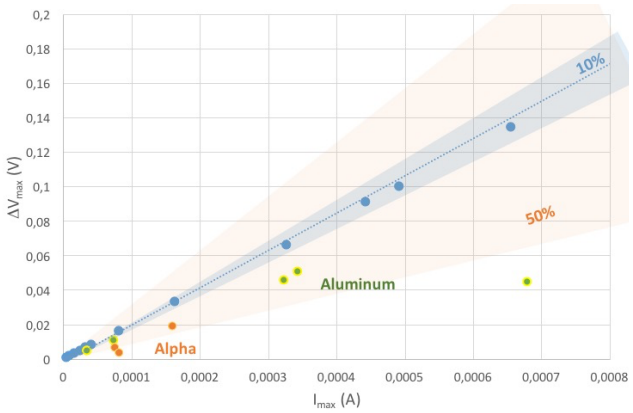

Fig. 28. Linearity curve and detected currents concerning the aluminum ion or the alpha particle crossing in a fifteen contacts matrix.

The metrics corresponding to these currents and voltages have been reported in Fig. 28. All the currents are correctly reproduced excepted the N10 current of the aluminum. This is surprising because this current is large enough to be correctly detected by the VCO. However, it is probably to high and its maximum value meets the saturation value of the VCO.

VI. Conclusion

The detection chain presented in this work is based on an innovative concept: an indirect particle detection through a voltage controlled oscillator. The analysis of the results extracted from this chain showed the possibility to recognize the input signal (from a given particle) by observing the average voltage of the output signal. The main advantage of this system is the possibility to get all the information related to the input signal (shape and order of magnitude of the current and duration) with a good sensitivity of detection.

In this paper, we have explored the possibility to improve the signal tracking by optimizing the detection matrix. Thus, the impact of the distance between contacts, their size and their number have been analyzed. Finally, with a VCO oscillating at 4.3GHz we demonstrate that tracking various kinds of particles is possible. It is also possible to link easily the characteristics of the input current to the output signal and then to get information about the detected particles. The last part of the study deals with the opportunity to link the currents collected at the contacts to the particles configuration. Then the maximum generation time gives information about the distance from the contact to the particle and the current peak can give information about the charge density. The total collected charge provides information about the deposited energy.

One interesting application for the VCO based detector could be spectrometry analysis. Then the oscillator frequency could be calibrated to select particles with various characteristics. In that case, several VCO working at different frequencies could be used, giving the opportunity to characterize accurately a given environment.

References

[1] C. Fiorini, A. Pullia, E. Gatti, A. Longoni, and W. Buttler, "A monolitic implementation of a switch-current 'wheel' amplifier for multi-channel silicon drift detectors, *IEEE Trans.* Nucl. Sci., vol. 46 n°3 p. 161, 1999.

[2] D. Hussona,, A. Bozierb, S. Higueretc, T.D. Lec, A. Nourreddinea, "AlphaRad, a new integrated CMOS System-on-Chip for high efficiency alpha particles counting" , *Nuclear Instruments and Methods in Physics Research A 569*., pp. 845-852 161, 2006.

[3] I. Perić, C. Kreidl, P. Fischer, "Particle pixel detectors in high-voltage CMOS technology–New achievements", Nuclear Instruments and Methods in Physics Research A, Vol. 650, Issue 1, p. 158-162, 2011.

[4] M. Trocmé, S. Higueret, D. Husson, A. Nourreddine, T.D. Lê, "A new compact device for efficient neutron counting using a CMOS active pixel sensor", Radiation Measurements, pp. 1100-1103, 2008.

[5] D. Passeri, P. Placidi, L. Verducci, P. Ciampolini, G. Matrella, A. Marras, G/M. Bilei, "High-resolution CMOS particle detectors: design and test issues", 331-334 Vol.1, *2003* IEEE Nuclear Science S*ymposium Conference Record*.

[6] M. Campbell, V. Havranek, E. HEIjne, T. Holy, J. Idarraga, J. Jakubek, C. Lebel, C. Leray, X. Llopart, J. Novotny, S. Pospisil, L. Tlustos, Z. Vykydal, "Charge collection from proton and alpha particle tracks in silicon pixel detector devices", 2007 IEEE Nuclear Science S*ymposium Conference Record.*

[7] M. J. Baudot ; G. Bertolone ; A. Brogna ; G. Claus ; C. Colledani et al., "First test results Of MIMOSA-26, a fast CMOS sensor with integrated zero suppression and digitized output", 2009 IEEE Nuclear Science S*ymposium Conference Record,* 2009.

[8] Tomas Baca ; Martin Jilek ; Petr Manek ; Petr Stibinger ; Vladimir Linhart ; Jan Jakubek ; Martin Saska, "Timepix Radiation Detector for Autonomous Radiation Localization and Mapping by Micro Unmanned Vehicles", 2019 IEEE/RSJ International Conference on Intelligent Robots and Systems (IROS), 3-8 Nov. 2019.

[9] Ying Zhang, Christine Hu-Guo, Daniel Husson, The-Duc Le , Stéphane Higueret, Yann Hu, "A High-Sensitivity Low-Power CMOS Sensor for a Future Neutron Personal Dosimeter", *in IEEE Trans. On Nucl. Sc.*, vol.59, no.4, pp. 1465-1471, August 2012.

[10] Rahajandraibe W., Aziza H., Coulié-Castellani K., Micolau, "Device and Method for Detecting Radiation Particles"
G. Patent AMU/CNRS/UAPV – Septembre 17, 2015 WO2015136220, https://patentscope.wipo.int/search/en/detail.jsf?docId=WO2015136220

[11] K. Castellani-Coulié, H. Aziza, W. Rahajandraibe, G. Micolau, J.-M. Portal, "Development of a CMOS Oscillator Concept for Particle Detection and Tracking", *IEEE Trans Nucl. Sci.*, Vol. 60 , Issue 4 , pp. 2450 - 2455 , Aug. 2013. DOI: 10.1109/TNS.2013.2254723

[12] K. Coulié-Castellani, W. Rahajandraibe, G. Micolau, H. Aziza, J.-M. Portal, "Improvement of a detection chain based on a VCO concept for microelectronic reliability under natural radiative environment", *IEEE LATW Conference*, 2015.

[13] S. Ben Krit, K. Coulié-Castellani, W. Rahajandraibe, L. Ottaviani, G. Micolau, H. Aziza, J.-M. Portal, "Comparison of a Readout Chain Dedicated to the Signal Conditioning of a Particle Detector and an Innovative Chain Based on a VCO Concept", *RADECS 2015*, Moscou, Russia, September 2015. DOI: 10.1109/RADECS.2015.7365592

[14] TCAD Sentaurus user's manual (Synopsys).

[15] A. Akkerman, J. Barak, D. Emfietzoglou, "Ion and electron track-structure and its effects in silicon: model and calculation", *Nuclear Instruments and Methods in Physics Research*, pp. 319-336, 2005.

[16] www.srim.org

[17] Vasiliy V. Markelov and Michael G. Tverskoy, "Evaluation of LET Spectra Produced by High Energy Protons in Si", *RADECS 2015*, Moscou, Russia, September 2015. DOI: 10.1109/RADECS.2015.7365592

[18] K. Coulié, W. Rahajandraibe, H. Aziza, G. Micolau, R. Vauché, "Detection limit of a VCO based detection chain dedicated to particles recognition and tracking", *2005 8th European Conference on Radiation and Its Effects on Components and Systems*, 2005. DOI: 10.1109/RADECS.2005.4365629.